Constraints on the upper crustal magma reservoir beneath Yellowstone Caldera inferred from lake-seiche induced strain observations

Karen Luttrell,[1] David Mencin,[2] Olivier Francis,[3] and Shaul Hurwitz[1]

Received 5 November 2012; revised 7 January 2013; accepted 10 January 2013.

[1] Seiche waves in Yellowstone Lake with a ~78-minute period and heights <10 cm act as a load on the solid earth observed by borehole strainmeters with subnanostrain sensitivity throughout the Yellowstone Caldera. The far-field strain induced by the load of the seiche waves calculated with a homogeneous elastic model representing the upper crust is more than an order of magnitude smaller than the measured strain amplitude ~30 km from the lake shore. By contrast, the observed far field strain amplitudes are consistent with the seiche load on a two-layered viscoelastic model representing an elastic upper crust overlying a partially molten body deeper than 3–6 km with Maxwell viscosity less than 10^{11} Pa s. These strain observations and models provide independent evidence for the presence of partially molten material in the upper crust, consistent with seismic tomography studies that inferred 10%–30% melt fraction in the upper crust. **Citation:** Luttrell, K., D. Mencin, O. Francis, and S. Hurwitz (2013), Constraints on the upper crustal magma reservoir beneath Yellowstone Caldera inferred from lake-seiche induced strain observations, *Geophys. Res. Lett.*, *40*, doi:10.1002/grl.50155

1. Introduction

[2] The Yellowstone Plateau Volcanic Field is characterized by abundant seismicity, ground deformation, and hydrothermal activity [e.g., *Chang et al*., 2007; *Farrell et al*., 2010; *Fournier*, 1989; *Lowenstern and Hurwitz*, 2008]. The activity is centered on the 640 ka Yellowstone Caldera where seismic tomography, crustal deformation, and gravity observations suggest partially molten magma at depths of up to 3–10 km [e.g., *Chang et al*., 2010; *Chu et al*., 2010; *DeNosaquo et al*., 2009; *Husen et al*., 2004; *Wicks et al*., 2006]. The characterization of the caldera subsurface, and the magma reservoir in particular, is an important and ongoing concern for evaluating hazard in the region [*Christiansen et al*., 2007].

[3] In late 2008, five borehole strainmeters (BSM) were installed in and around the Yellowstone Caldera (Figure 1), as part of the Plate Boundary Observatory (PBO) geodetic network expansion [*Hodgkinson et al*., 2013]. BSM can resolve horizontal strains of less than 10^{-9} (nanostrain), which is equivalent to detecting a micron of length change over a distance of a kilometer. When calibrated, BSM data represent the three components of the horizontal strain tensor in the East-North coordinate system: areal strain (ε_A), differential strain (ε_D), and engineering shear strain (ε_S) (Supporting Information, S1). Two BSM were installed on the shores of Yellowstone Lake, a large (~30 km by 20 km) irregularly shaped freshwater lake that straddles the southeastern boundary of the caldera, and another three BSM were installed ≤30 km away near the northern edge of the caldera.

[4] In this study, we demonstrate that subtle seiche waves in Yellowstone Lake that are recorded by pressure transducers [*Mencin et al*., 2012] produce observable crustal strain at distances of at least 30 km. By modeling these strain signals, we constrain the subsurface rheology within the Yellowstone caldera using observations that are independent from previous studies. In particular, we estimate the viscosity and upper depth of a partially molten magma body.

2. Seiche Observations

[5] In July 2009, network operators at UNAVCO doing routine station data inspections noticed a remarkable signal with a period of 78 minutes and an amplitude comparable in size to the earth tide in data from B944 (Figure S1) [*Mencin et al*., 2010]. The transient signal began suddenly, maintained strong amplitude for the next 12 hours, and then gradually decayed over the next few days. Further inquiry revealed that a signal of the same period, although with a smaller amplitude, was also present at stations B205 and B206, which are ~30 km away from the lake (Figure 1). It was soon recognized that the onset of the signal coincided with a high amplitude periodic disturbance of the lake measured by a gauge on the Yellowstone River at the lake outlet (Figure 1). This led to the hypothesis that large waves had formed on the lake surface and that the load of those waves was causing the observed deformation at the BSM around the caldera. The remarkably steady long-period nature of the signal is consistent with a standing seiche wave that resonates across the lake basin [*Mencin et al*., 2012].

[6] These transient periodic signals occur year round, even when the lake is frozen in the winter. The waves can be either impulse-like (beginning suddenly and gradually decaying over days) or emergent (gradually building over days, sustained at high amplitude for days, and then decaying over days) but always with the same remarkably steady period. Seiche signals have also been recorded on two colocated tiltmeters in boreholes B944 and B208. Lake basin models suggest that the 78-minute period is consistent with water mass transfer between the West Thumb and Southeast Arm Basins (Figure S2, Supporting Information S2).

[7] To better quantify seiche amplitude, an absolute pressure gauge (APG) was deployed in West Thumb (Figure 1) in four separate campaigns during 2011–2012, each lasting between 3 and 10 weeks for a total of 20 weeks (Table

All Supporting Information may be found in the online version of this article.

[1]U. S. Geological Survey, Menlo Park, California, USA.
[2]UNAVCO, Boulder, Colorado, USA.
[3]Université du Luxembourg, Luxembourg, Luxembourg.

Corresponding author: Karen Luttrell, U. S. Geological Survey 345 Middlefield Rd. MS 910, Menlo Park, CA 94025, USA. (kluttrell@usgs.gov)

0094-8276/13/10.1002/grl.50155

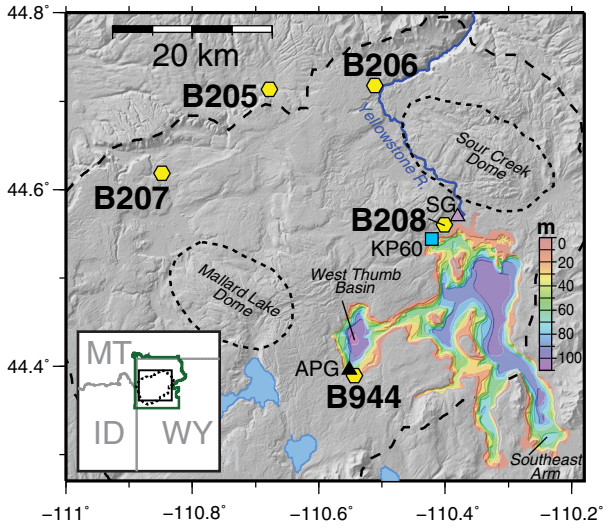

Figure 1. Map of study region. Yellowstone Lake bathymetry from the study by *Morgan et al*. [2007]. Yellow hexagons indicate borehole strainmeters. Black and purple triangles indicate locations of absolute pressure gauge (APG) and stream gauge (SG), respectively. Blue square indicates location of weather station KP60. Solid green line (inset) indicates Yellowstone National Park boundary, and dashed lines indicate approximate boundary of the Yellowstone caldera and the two resurgent domes.

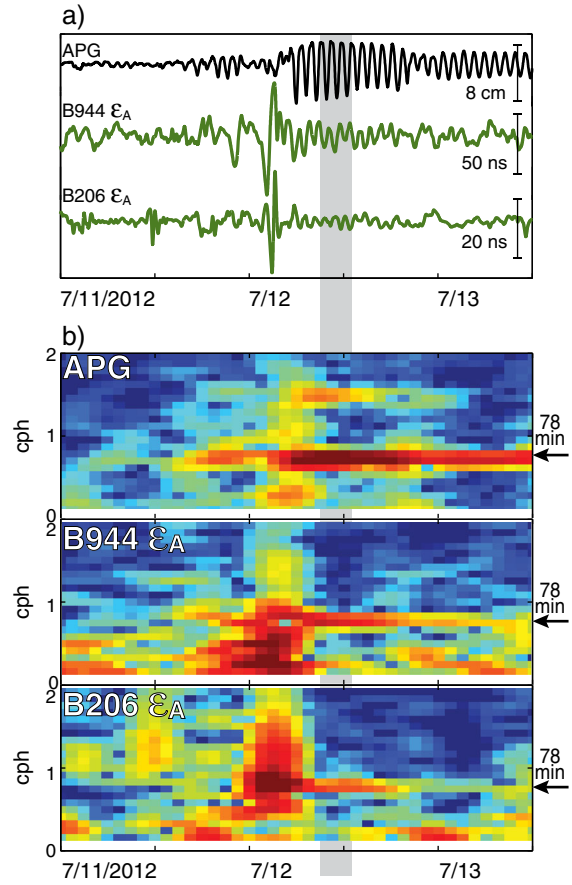

Figure 2. (a) Seiche signals recorded between 11 and 13 July 2012 on APG (top), B944 areal strain (middle), and B206 areal strain (bottom). All time series band pass filtered between 8 hours and 20 minutes. (b) Spectrogram of APG (top), B944 areal strain (middle), and B206 areal strain (bottom). Frequency is in cycles per hour (left axis), with 78-minute period indicated at the right. Gray box indicates measurement time window (Figures S3 and S4). Measured amplitude during this time is listed in Table 1.

S1). During these periods, 17 seiche events were measured on the APG and on strainmeters B944 and B206 (B205, B207, and B208 were nonfunctional during this period). The amplitudes of seiche waves recorded by the APG range from 1.5 to 8 cm, peak to trough. Strain amplitudes at B944 during these times range from 5 to 22 ns ε_A, 6 to 20 ns ε_D, and 8 to 45 ns ε_S, and at B206 amplitudes range from 1 to 4.5 ns ε_A, 1 to 2.5 ns ε_D, and 2 to 8 ns ε_S. In general, the strain signal observed at B206 is about an order of magnitude less than that observed at B944. Strain amplitude generally correlates well with the lake amplitude, particularly at B944, the station closest to the lake.

[8] The largest seiche during the period of APG deployment occurred on 12 July 2012 (Figure 2 and Supporting Information S3). Spectrograms show a sudden increase in energy at the time of seiche wave onset followed by strong resonant energy at a period of 78 minutes. To model the deformation induced by this seiche wave, we first precisely determined the range of peak-to-trough amplitudes observed during a 4-hour window following the initial seiche impulse. The range of amplitudes observed during this time is the "measured range" (Table 1), while the “effective range” also includes a 25% uncertainty resulting from BSM calibration (Table 1, Supporting Information S1). There is no observed delay in onset time between the seiche recorded at the APG and the BSM, and the phase lag between the APG and BSM is 26 ± 10 minutes (Supporting Information S3). As such, we determine that seiche-related deformation at B944 and B206 is observed within 25 minutes of the associated seiche load.

3. Models of the Seiche-induced Strainfield

[9] The novel observation that seiche waves in Yellowstone Lake induce observable strain signals 30 km from the lake presents us with a natural experiment for analyzing the caldera subsurface properties. We rule out the possibility that stress transfer is caused by pore pressure diffusion because of the short timescales involved and instead model deformation resulting from the weight of the water load on the solid earth. We consider two models with different rheologies that could

Table 1. Amplitude of seiche wave oscillations observed on 12 July 2012

APG	*Measured range*[a]	
Lake height (cm)	7-8	
B944	*Measured range*[a]	*Effective range*[b]
EA (ns)	14.0-22.0	10.5-27.5
ED (ns)	14.0-18.5	10.5-23.1
ES (ns)	36.0-49.0	27.0-61.3
B206	*Measured range*[a]	*Effective range*[b]
EA (ns)	2.5-4.5	1.8-5.6
ED (ns)	1.0-1.5	0.8-1.9
ES (ns)	2.9-4.3	2.2-5.4

[a]Range measured during four-hour window on 12 July 2012 09:00–13:00 UTC (Figure S5).
[b]Measured range ±25% to account for possible calibration process error (Supporting Information S3).

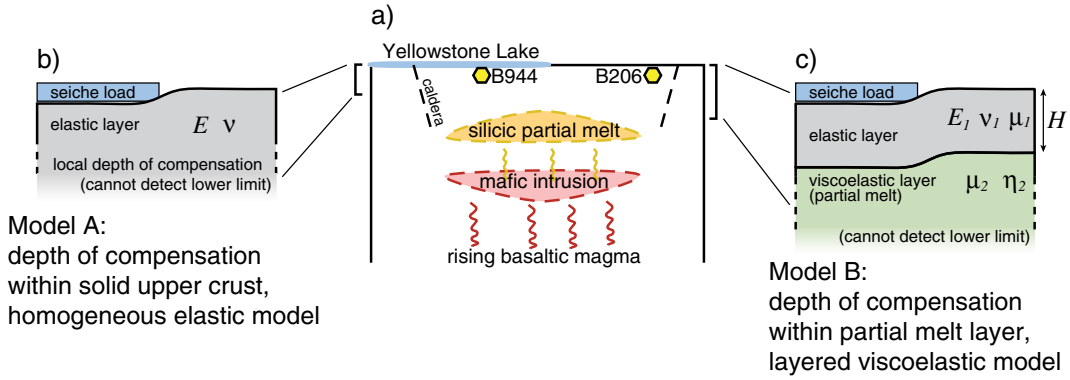

Figure 3. (a) Schematic cross section of Yellowstone caldera [after *Lowenstern and Hurwitz*, 2008], with approximate locations of Yellowstone Lake and BSM. (b) Model A assumes lake seiche load is fully compensated within an elastic upper crust. (c) Model B assumes lake seiche load is compensated by an elastic upper crust above a partial melt. Models are not sensitive to properties of material below the local depth of compensation of the seiche load.

produce a strain response within 25 minutes at both close and distant locations (Figure 3). In both models, we try to determine the effective local depth of compensation of the small seiche load, below which the stress field is unperturbed. The amplitude and timing of the observed strain signals are only influenced by the material properties above this depth of compensation.

[10] The first model (Model A) assumes that the local depth of compensation is in the solid shallow crust and is represented by a uniform elastic half-space (Figure 3b). The second model (Model B) assumes that the local depth of compensation is within a layer of partial melt in the caldera, possibly including aqueous-rich fluids, represented by a viscoelastic half-space underlying an elastic layer (Figure 3c). The error from excluding the effect of the lateral and lower boundaries of a partial melt layer is second order compared with the uncertainty in the observations. For both models, we calculate the strain field in response to a peak-to-trough seiche wave load (Figure S2, Supporting Information S2) using a semi-analytic method, which convolves the real 2-D shape of the surface load with a vertical Green's function describing the response of the subsurface to a point load [e.g., *Luttrell and Sandwell*, 2010; *Smith and Sandwell*, 2003; 2004] using a range of material properties. We then compare the predicted strainfield with the measured and estimated strain components at B206. Because B944 is very close to the load edge, the strain gradient is very high. As such, small scale variations in load shape or material properties not included in these models will have a much greater effect at B944 compared with B206. We therefore use only observations from B206 to evaluate models A and B.

[11] A cold dry rhyolite will generally have a young's modulus of 40–70 GPa and a Poisson's ratio of 0.2–0.25 [e.g., *Turcotte and Schubert*, 2002]. In Yellowstone Caldera, the lithology is primarily of rhyolitic composition and may be thermally weakened [*Christiansen*, 2001]. As such, for the upper layer, we consider a homogeneous elastic material with a Young's modulus (E) between 1 and 50 GPa and a Poisson's ratio (ν) between 0 and 0.5. Model A is fully described by these two parameters. For Model B, we assume that the bulk modulus of the elastic and viscoelastic layers is the same, such that Model B can be described with four free parameters: E_1 and ν_1 describing the upper elastic layer, the depth to the interface H, and ratio of the shear moduli of the lower and upper layers μ_2/μ_1, which is related to the viscosity of the lower layer. (A ratio of $\mu_2/\mu_1 = 1$ is the same as the elastic half-space solution, while $\mu_2/\mu_1 = 0$ indicates the lower layer is an idealized fluid of negligible viscosity).

[12] The range of strain component amplitudes predicted by Model A is summarized in Figure S6, along with map-view and cross-section depictions of the areal strainfield of one such model. The results from Model B are similarly summarized in Figure 4. Within the range of examined parameters, Model A is never consistent with either the measured (thin line) or effective (thick line) ranges of all three strain components at B206 (Figure S6a, Table 1). Even in a very weak crust ($E < 5$ GPa), the predicted strain amplitude decays significantly within a few kilometers of the lake (Figure S6 b and c) and produces minimal deformation at the location of B206. This suggests that the seiche-induced load represented by the relatively high amplitude strains observed at B206 cannot be entirely supported within an elastic upper crust.

[13] Model B, on the other hand, can successfully reproduce the effective amplitude range of both the measured (thin lines, black shading) and effective (thick lines, gray shading) strain components at B206 using a range of plausible model parameters (Figures 4a and 4b). The results are consistent with a Young's modulus $E_1 \leq 30$ GPa, and a shear modulus ratio $\mu_2/\mu_1 \leq 0.05$; Poisson's ratio (ν_1) is unconstrained by this analysis. Plate thickness (H) is the most sensitive parameter and can be constrained within a range of 3–6 km. This range is indicative of the uncertainty in the location of the top of the viscoelastic layer, but the depth to the bottom of the viscoelastic layer is undetectable by this analysis as it lies below the local depth of compensation for the seiche load. An example of one nonunique calculated areal strainfield that satisfies the observations is shown in Figures 4c and 4d.

4. Discussion and Conclusions

[14] While uncertainties remain in our estimates of both the seiche amplitude and the strain response, and our models incorporate many simplifying assumptions, some conclusions can be drawn from the model results. First, the observed strainfield associated with seiche loading is definitely sensitive to partially fluid material in the subsurface. Second, the results of Model B provide observational upper bounds on the elastic

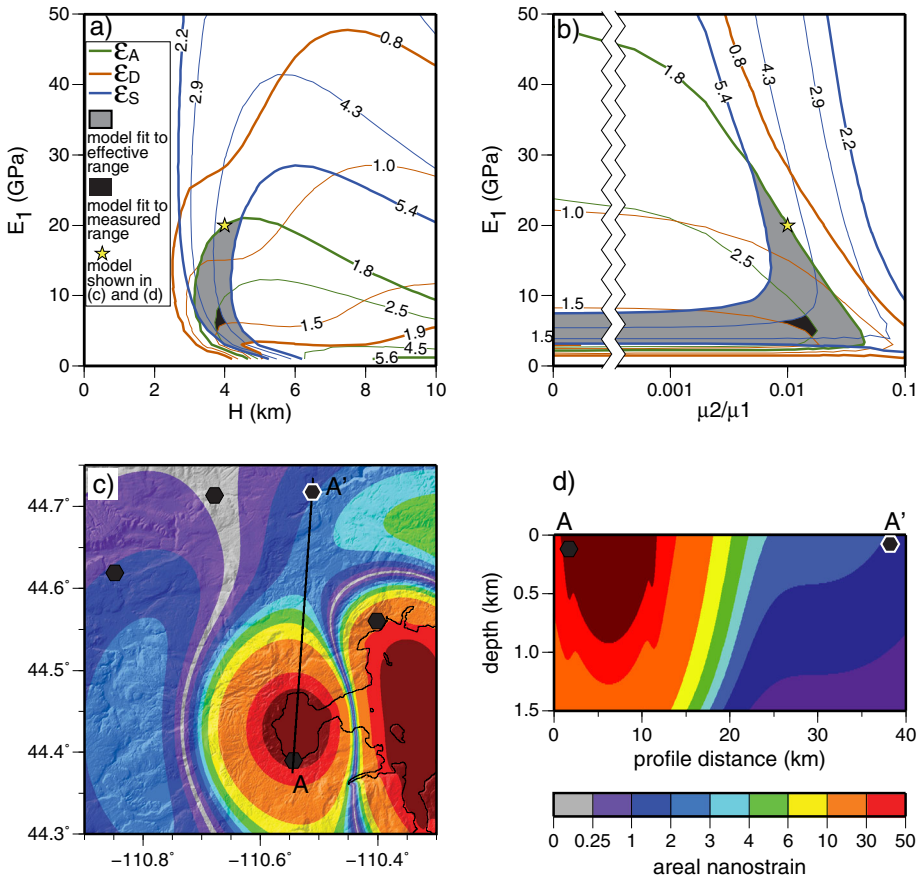

Figure 4. Contours of modeled strain amplitude in a layered viscoelastic crust (Figure 3c) at BSM site B206. (a) Strain as a function of model parameters E_1 and H with constant $\mu_2/\mu_1 = 0.01$, and (b) as a function of E_1 and μ_2/μ_1 with constant $H = 4$ km. Areal (green), differential (brown), and engineering shear (blue) components shown. Contour values are measured range (thin lines) and effective range (thick lines) of B206 strain components (Table 1). Gray- and black-shaded regions indicate range of model parameter space able to fit effective and measured strain component observations, respectively. Star indicates modeled strainfield shown in Figures 4c and 4d). (c) Modeled areal strain field at depth of B206 (78 m). Black hexagons indicate BSM locations, with white outline designating B206. (d) Modeled areal strainfield along profile A-A'.

properties of the Yellowstone Caldera upper crust. Currently, very few observational constraints exist for the appropriate strength parameters for the shallow crust in volcanic regions and previous Yellowstone Caldera deformation studies have instead used laboratory-derived estimates of the Young's or shear moduli for cold dry granitic rock [e.g., *Chang et al.*, 2007; *Waite and Smith*, 2002]. However, when interpreting crustal deformation related to a possible magmatic intrusion, the use of context-appropriate parameter values is particularly important because they strongly influence model results [e.g., *Newman et al.*, 2006]. The upper bounds on Young's modulus and shear modulus ratio derived from Model B correspond to an upper shear modulus $\mu_1 \leq 15$ GPa and a lower shear modulus $\mu_2 \leq 0.75$ GPa.

[15] Through standard relations, these constraints on elastic moduli can be further related to a seismic P-wave velocity reduction (Δv_P) of up to 35% and a shear wave velocity reduction (Δv_S) of at least 80%. This is higher than the reduction reported by *Husen et al.* [2004] (6% Δv_P) attributed to 8%–15% melt fraction and is closer to the velocity reductions reported by *Chu et al.* [2010] (66% Δv_S) attributed to 32% melt fraction and those reported for more localized regions beneath the resurgent domes (30% Δv_P) [*Lehman et al.*, 1982; *Miller and Smith*, 1999] attributed to 10%–50% melt fraction. This approximate agreement is remarkable considering this study uses completely independent observations.

[16] Additionally, our temporal observations lead to constraints on the viscosity of the lower layer. The shear modulus μ of a Maxwell viscoelastic solid is related to the viscosity η via the characteristic Maxwell relaxation time τ_m as $\eta = \tau_m \mu/2$. In such a material, relaxation is generally complete after ~4 τ_m [*Luttrell et al.*, 2007]. Our observation that seiche-induced strain signals at B944 and B206 occur within 25 minutes of the seiche load at the APG corresponds to $\tau_m \leq 6$ minutes. When combined with the constraints on E_1 and μ_2/μ_1, this indicates that the viscosity of the lower layer (η) is $<10^{11}$ Pa s. A fully molten rhyolitic magma has a viscosity ~10^5–10^8 Pa s, while the viscosity of rhyolite rocks near their melting point is ~10^{16} Pa s [*Ardia et al.*, 2008]. This implies that the lower layer is partially molten and is inconsistent with the gradual ductile deformation of rocks near their melting point. The viscosity of a multiphase magma depends upon many factors such as composition, temperature, water content, strain rate, and crystal fraction [e.g., *Petford*, 2003 and references therein]. In a Yellowstone caldera rhyolite, a viscosity less than 10^{11} Pa s likely corresponds to a mush with at least 35% melt fraction, although this fraction may be much smaller if the

melt has a very high volatile content (e.g., water content much greater than 2 wt%).

[17] Seismic tomography studies have imaged a large ($>$1000 km^3) low-velocity body beneath much of the caldera with upper extents as shallow as 6 km [*Miller and Smith*, 1999], 8 km [*Husen et al*., 2004], and 3 km [*Chu et al*., 2010]. This body is interpreted as partially molten rhyolitic magma consisting of 10%–30% melt [*Chu et al*., 2010; *Lehman et al*., 1982; *Smith et al*., 2009]. Petrochemical constraints [*Girard and Stix*, 2012], crustal deformation studies [*Chang et al*., 2010; *Chang et al*., 2007], and gravity observations [*DeNosaquo et al*., 2009] are similarly consistent with a partially molten body beneath 7–10 km depth. The depth constraint on the top of partial melt of 3–6 km from this study is consistent with the shallowest estimates from previous studies, although with potentially higher melt fraction. However, because the strainfield associated with the seiche load is only sensitive to the portion of crust above the local depth of compensation, it can offer no constraints on the volume of the compensating body. As such, it is possible that the parameters we estimate represent the top of the large magma reservoir imaged in previous studies, but it is also possible that they instead represent the properties of a smaller network of melt pockets that lie above a deeper large magma reservoir and would be too small to be observed using tomographic techniques with multikilometer scale resolution [*Lowenstern et al*., 2006]. This study is only sensitive to the shallowest occurrence of low-viscosity material.

[18] A recent earthquake swarm beneath Yellowstone Lake has been interpreted to result from shallow magmatic intrusions [*Farrell et al*., 2010], and there have also been indications that magma may be present closer to the surface beneath the Sour Creek resurgent dome, compared with other areas in the caldera [e.g., *Chang et al*., 2010; *Wicks et al*., 2006]. Because the strain signal at B206 is most sensitive to the properties of the crust between it and the lake, the proximity of these shallow melt bodies would strongly influence our estimates of the depth and viscosity of partial melt. The constraints on subsurface properties described in this study may be made more robust if observations from additional locations become available, such as at B205, B207, and B208. The continued observation of Yellowstone Lake and the Yellowstone Caldera strainfield can contribute valuable information to the understanding and monitoring of the Yellowstone magmatic system.

[19] **Acknowledgments.** We thank Kathleen Hodgkinson, Stacey Kinsey, and Henry Heasler for their assistance in collecting the observations used in this study. We thank Dave Hill, Jacob Lowenstern, John Langbein, Tony Lowry, and Wu-Lung Chang for helpful reviews. Borehole strainmeter observations are collected as part of the Plate Boundary Observatory project of the Earthscope program of the National Science Foundation and are managed by UNAVCO. Stream discharge measurements in the Yellowstone River are maintained by USGS. Absolute pressure gauge in Yellowstone Lake is maintained by UNAVCO. Data from weather station KP60 is provided by NCDC. This research was supported by the USGS Mendenhall and Volcano Hazards programs.

References

Ardia, P., D. Giordano, and M. W. Schmidt (2008), A model for the viscosity of rhyolite as a function of H2O-content and pressure: A calibration based on centrifuge piston cylinder experiments, *Geochemica et Cosmochimica Acta*, *72*, 6103–6123, doi:10.1016/j.gca.2008.6108.6025.

Chang, W. L., R. B. Smith, J. Farrell, and C. M. Puskas (2010), An extraordinary episode of Yellowstone caldera uplift, 2004–2010, from GPS and InSAR observations, *Geophys. Res. Lett.*, *37*(L23302), doi:10.1029/2010GL045451.

Chang, W. L., R. B. Smith, C. Wicks, J. M. Farrell, and C. M. Puskas (2007), Accelerated uplift and magmatic intrusion of the Yellowstone caldera, 2004 to 2006, *Science*, *318*(5852), 952–956, doi:10.1126/Science.1146842.

Christiansen, R. L. (2001), The Quaternary and Pliocene Yellowstone Plateau Volcanic Field of Wyoming, Idaho, and Montana, *U.S. Geological Survey Professional Paper*, *729-G*, USGS Information Services, Denver, CO.

Christiansen, R. L., J. B. Lowenstern, R. B. Smith, H. Heasler, L. A. Morgan, M. Nathenson, L. G. Mastin, L. J. P. Muffler, and J. E. Robinson (2007), Preliminary Assessment of Volcanic and Hydrothermal Hazards in Yellowstone National Park and Vicinity, *U.S. Geological Survey Open-File Report*, *2007–071*, 94 pp.

Chu, R., D. V. Helmberger, D. Sun, J. M. Jackson, and L. Zhu (2010), Mushy Magma beneath Yellowstone, *Geophys. Res. Lett.*, *37*(L01306), doi:10.1029/2009GL041656.

DeNosaquo, K. R., R. B. Smith, and A. R. Lowry (2009), Density and lithospheric strength models of the Yellowstone-Snake River Plain volcanic system from gravity and heat flow data, *J. Volcano. Geotherm. Res.*, *188* (1–3), 108–127, doi:10.1016/J.Jvolgeores.2009.08.006.

Farrell, J., R. B. Smith, T. Taira, W. L. Chang, and C. M. Puskas (2010), Dynamics and rapid migration of the energetic 2008–2009 Yellowstone Lake earthquake swarm, *Geophys. Res. Lett.*, *37*(L19305), doi:10.1029/2010GL044605.

Fournier, R. O. (1989), Geochemistry and Dynamics of the Yellowstone-National-Park Hydrothermal System, *Ann. Rev. Earth Planet. Sci.*, *17*, 13–53.

Girard, G., and J. Stix (2012), Future volcanism at Yellowstone caldera: Insights from geochemistry of young volcanic units and monitoring of volcanic unrest, *GSA Today*, *22*(9), doi:10.1130/GSATG1143A.1131.

Hodgkinson, K. M., J. Langbein, B. Henderson, D. Mencin, and A. A. Borsa (2013), Tidal calibration of plate boundary obervatory borehole strainmeters, *J. Geophys. Res.*, *in press*, doi:10.1029/2012JB009651.

Husen, S., R. B. Smith, and G. P. Waite (2004), Evidence for gas and magmatic sources beneath the Yellowstone volcanic field from seismic tomographic imaging, *J. Volcano. Geotherm. Res.*, *131*(3–4), 397–410, doi:10.1016/S0377-0273(03)00416-5.

Lehman, J. A., R. B. Smith, and M. W. Schilly (1982), Upper crustal structure of the Yellowstone Caldera from seismic delay time analyses and gravity correlations, *J. Geophys. Res.*, *87*(B4), 2713–2730.

Lowenstern, J. B., and S. Hurwitz (2008), Monitoring a supervolcano in repose: Heat and volatile flux at the yellowstone caldera, *Elements*, *4*(1), 35–40, doi:10.2113/Gselements.4.1.35.

Lowenstern, J. B., R. B. Smith, and D. P. Hill (2006), Monitoring supervolcanoes: geophysical and geochemical signals at Yellowstone and other large caldera systems, *Phil. Trans. R. Soc. A*, *364*, 2055–2072, doi:2010.1098/rsta.2006.1813.

Luttrell, K., and D. Sandwell (2010), Ocean loading effects on stress at near shore plate boundary fault systems, *J. Geophys. Res.*, *115*, B08411, doi:10.1029/2009jb006541.

Luttrell, K., D. Sandwell, B. Smith-Konter, B. Bills, and Y. Bock (2007), Modulation of the earthquake cycle at the southern San Andreas fault by lake loading, *J. Geophys. Res.*, *112*, B08411, doi:10.1029/2006JB004752.

Mencin, D., S. Hurwitz, K. Hodgkinson, M. Jackson, and A. Borsa (2010), Observations of Seiches in the Yellowstone Caldera, EGU General Assembly, Vienna, Austria, 2-7 May, Paper 11324.

Mencin, D., K. Luttrell, O. Francis, K. Hodgkinson, J. Lente, and S. Hurwitz (2012), Unique and remarkable observations of Seiche behavior in Lake Yellowstone, *EOS Trans. AGU, Fall Meet. Suppl.*, *Abstract V13B*-2851.

Miller, D. S., and R. B. Smith (1999), P and S velocity structure of the Yellowstone volcanic field from local earthquake and controlled-source tomography, *J. Geophys. Res.*, *104*(B7), 15105–15121.

Morgan, L. A., W. C. Shanks, G. K. Lee, and M. W. Webring (2007), Bathymetry and geology of the floor of Yellowstone Lake, Yellowstone National Park, Wyoming, Idaho, and Montana, *U.S. Geological Survey Scientific Investigations Map*, *2973*, 2 sheets.

Newman, A. V., T. H. Dixon, and N. Gourmelen (2006), A four-dimensional viscoelastic deformation model for Long Valley Caldera, California, between 1995 and 2000, *J. Volcan. Geotherm. Res.*, *150*, 244–269, doi:210.1016/j.jvolgeores.2005.1007.1017.

Petford, N. (2003), Rheology of Granitic Magmas During Ascent and Emplacement, *Annu. Rev. Earth Planet. Sci.*, *31*, 399–427, doi:310.1146/annurev.earth.1131.100901.141352.

Smith, B., and D. Sandwell (2003), Coulomb stress accumulation along the San Andreas Fault System, *J. Geophys. Res.*, *108*(B6), 2296.

Smith, B., and D. Sandwell (2004), A three-dimensional semianalytic viscoelastic model for time-dependent analyses of the earthquake cycle, *J. Geophys. Res.*, *109*, B12401, doi:10.1029/2004JB003185.

Smith, R. B., M. Jordan, B. Steinberger, C. M. Puskas, J. Farrell, G. P. Waite, S. Husen, W. L. Chang, and R. O'Connell (2009), Geodynamics of the Yellowstone hotspot and mantle plume: Seismic and GPS imaging, kinematics, and mantle flow, *J. Volcano. Geotherm. Res.*, *188*(1–3), 26–56, doi:10.1016/J.Jvolgeores.2009.08.020.

Turcotte, D. L., and G. Schubert (2002), *Geodynamics*, Cambridge University Press. Cambridge, UK

Waite, G. P., and R. B. Smith (2002), Seismic evidence for fluid migration accompanying subsidence of the Yellowstone caldera, *J. Geophys. Res.*, *107*(B9), doi:10.1029/2001JB000586.

Wicks, C. W., W. Thatcher, D. Dzurisin, and J. Svarc (2006), Uplift, thermal unrest and magma intrusion at Yellowstone caldera, *Nature*, *440* (7080), 72–75, doi:10.1038/Nature04507.